PAPER: CLASSICAL STATISTICAL MECHANICS, EQUILIBRIUM AND NON-EQUILIBRIUM

Jamming and percolation in random sequential adsorption of straight rigid rods on a two-dimensional triangular lattice

Journal of Statistical Mechanics: Theory and Experiment
An IOP and SISSA journal

PAPER: Classical statistical mechanics, equilibrium and non-equilibrium

Jamming and percolation in random sequential adsorption of straight rigid rods on a two-dimensional triangular lattice

E J Perino[1], D A Matoz-Fernandez[2], P M Pasinetti[1] and A J Ramirez-Pastor[1]

[1] Departamento de Física, Instituto de Física Aplicada (INFAP), Universidad Nacional de San Luis—CONICET, Ejército de los Andes 950, D5700HHW, San Luis, Argentina
[2] Division of Molecular Microbiology, School of Life Sciences, University of Dundee, Dundee DD1 5EH, United Kingdom
E-mail: mpasi@unsl.edu.ar

Received 19 April 2017
Accepted for publication 8 June 2017
Published 18 July 2017

Online at stacks.iop.org/JSTAT/2017/073206
https://doi.org/10.1088/1742-5468/aa79ae

Abstract. Monte Carlo simulations and finite-size scaling analysis have been performed to study the jamming and percolation behavior of linear k-mers (also known as rods or needles) on a two-dimensional triangular lattice of linear dimension L, considering an isotropic RSA process and periodic boundary conditions. Extensive numerical work has been done to extend previous studies to larger system sizes and longer k-mers, which enables the confirmation of a nonmonotonic size dependence of the percolation threshold and the estimation of a maximum value of k from which percolation would no longer occur. Finally, a complete analysis of critical exponents and universality has been done, showing that the percolation phase transition involved in the system is not affected, having the same universality class of the ordinary random percolation.

Keywords: critical exponents and amplitudes, finite-size scaling, irreversible aggregation phenomena, percolation problems

Supplementary material for this article is available online

1742-5468/17/073206+15$33.00

Contents

1. Introduction

Adsorption of extended objects is currently a very active field of research in physics, chemistry and biology. Deposition processes in which the relaxation over typical observation times is negligible can be studied as random sequential adsorption (RSA). In RSA processes, particles are randomly, sequentially and irreversibly deposited onto a substrate without overlapping each other. The quantity of interest is the fraction of lattice sites covered at time t by the deposited particles $\theta(t)$. Due to the blocking of the lattice by the already randomly deposited objects, the final state generated by RSA is a disordered state (known as jamming state θ_J), in which no more elements can be deposited due to the absence of free space of appropriate size and shape, $\theta_J \equiv \theta(t \to \infty) < 1$. This phenomenon plays an important role in numerous systems where the deposition process is irreversible over time scales of physical interest [1–6].

When a fraction θ of the lattice is covered by particles, nearest-neighbor occupied sites form structures called clusters. If the concentration of the deposited objects is large enough, a cluster of nearest-neighbor occupied sites extends from one side to the other of the lattice. The minimum concentration of sites for which this phenomenon occurs is named the percolation threshold θ_p, and determines a phase transition in the system [7–11]. As discussed in previous paragraph, θ ranges from 0 to θ_J for extended objects (i.e. objects occupying more than one lattice site) and the interplay between jamming and percolation must be considered.

Despite the simplicity of its definition, it is well-known that it is a quite difficult matter to analytically determine the value of the jamming coverage and percolation threshold. For some special types of lattices, geometrical considerations enable to derive their jamming and percolation thresholds exactly, i.e. one-dimensional (1D) substrates [12], and random bond percolation on square lattices (or, equivalently, random site percolation on triangular lattices) [8, 11].

https://doi.org/10.1088/1742-5468/aa79ae

J. Stat. Mech. (2017) 073206

In the case of lattice models of extended objects deposited on 2D lattices, which is the topic of this paper, the inherent complexity of the system still represents a major difficulty to the development of accurate analytical solutions, and computer simulations appear as a very important tool for studying this subject. In this line, it is worth mentioning some early works using dimers (objects occupying two adjacent sites on the lattice). Among them, Bunde *et al* [13] and Harder *et al* [14] investigated the percolating properties of dimeric phases in adsorption/diffusion systems; Evans [15] studied some problems of correlated percolation on Bethe lattices; and Evans and Sanders [16] used correlated percolation theory to analyze the propagation of the $c(2 \times 2)$ structure[3] in nonequilibrium adsorption models. However, in these papers, the evolution with the size of the objects was not explored, being limited exclusively to dimers and to small system sizes.

More recently, several authors investigated the deposition of linear k-mers or rods (objets occupying k consecutive sites in a row) on a two-dimensional (2D) square lattice [17–22]. The results obtained revealed that: (1) the jamming coverage decreases monotonically approaching the asymptotic value of $\theta_J = 0.66(1)$ for large values of k; (2) the percolation threshold of the occupied sites is a nonmonotonic function of the size k: it decreases for small rod sizes, goes through a minimum around $k = 13$, and finally increases for large segments; and (3) the ratio of the two thresholds θ_p/θ_J has a complex behavior: after initial growth, it stabilizes between $k = 3$ and $k = 7$, and then it grows again.

It is interesting to mention that a similar nonmonotonic behavior of the percolation threshold has been observed in previous studies of cooperative RSA (see [2], p 1318, and references therein). Here, the percolation threshold initially decreases with increasing the characteristic length (as expected given the introduction of clustering), passes through a minimum, and finally asymptotically converges towards the continuum regime limit.

There has been much less progress in addressing the RSA of extended objects on 2D triangular lattices [23–26]. In this line, Budinski-Petković and Kozmidis-Luburić [23] examined the kinetics of the RSA of objects of various shapes on a planar triangular lattice. The coverage of the surface and the jamming limits were calculated by Monte Carlo simulation. In all cases, the authors found that the jamming coverage decreases monotonically as the k-mer size increases: $\theta_J = \theta_0 + \theta_1 \exp(-k/r)$, where θ_0, θ_1 and r are parameters that depend on the shape of the adsorbing object. In the case of straight rigid k-mers, the simulations were performed for values of k between 1 and 11 and lattice size $L = 128$.

Later, Budinski-Petković *et al* [24] investigated percolation and jamming thresholds for RSA of extended objects on triangular lattices. Numerical simulations were performed for lattices with linear size up to $L = 1000$, and objects of different sizes and shapes (linear segments; angled objects; triangles and hexagons). It was found that for elongated shapes the percolation threshold monotonically decreases, while for more compact shapes it monotonically increases with the object size. In the case of compact objects such as triangles and hexagons, a no-percolation regime was observed. In the case of linear segments with values of k up to 20, the obtained results revealed that

[3] This phase could be associated with the RSA problem of particles with nearest-neighbor (NN) exclusion on a square lattice.

(1) the jamming coverage monotonically decreases with k, and tends to 0.56(1) as the length of the rods increases; (2) the percolation threshold decreases for shorter k-mers, reaches a value $\theta_p \approx 0.40$ for $k = 12$, and, it seems that θ_p does not significantly depend on k for larger k-mers; and (3) consequently, the ratio θ_p/θ_J increases with k.

The effects of anisotropy [25] and the presence of defects on the lattice [26] were also studied by the group of Budinski-Petković *et al* In summary, despite over two decades of intensive work, the current conjectures for the behavior of the percolation threshold and jamming concentration as a function of k are based on simulations for relatively short k-mers (up to $k = 20$). In this context, the main objective of the present paper is to extend the work of Budinski-Petković *et al* [23–26] to larger lattice sizes and longer k-mers. For this purpose, extensive numerical simulations (with $2 \leqslant k \leqslant 256$ and $40 \leqslant L/k \leqslant 160$) supplemented by analysis using finite-size scaling theory have been carried out. Our study allows (1) to obtain more accurate values of site percolation and jamming thresholds; (2) to improve the predictions on the behavior of the system for long rods; and (3) to perform a complete analysis of critical exponents and universality.

The paper is organized as follows: the model is described in section 2. The kinetics and jamming coverage are studied in section 3. The percolation properties are presented in section 4: simulation scheme, section 4.1; dependence of the percolation threshold on the size k, section 4.2; and analysis of the critical exponents and universality class, section 4.3. Finally, conclusions are given in section 5.

2. Model

Let us consider the substrate represented by a 2D triangular lattice of M $(= L \times L)$ sites with periodic boundary conditions in each direction, so that all the lattice sites are equivalent. In the filling process, straight rigid k-mers (with $k \geqslant 2$) are deposited randomly, sequentially and irreversibly on an initially empty lattice. This procedure, known as random sequential adsorption, is as follows: (i) one of the three (x_1, x_2, x_3) possible lattice directions and a starting site are randomly chosen; (ii) if, beginning at the chosen site, there are k consecutive empty sites along the direction selected in (i), then a k-mer is deposited on those sites (the k sites are marked as occupied). Otherwise, the attempt is rejected. When N rods are deposited, the concentration is $\theta = kN/M$. Figure 1(a) shows the formation of a percolating cluster (highlighted in blue) for a system of trimers (solid circles) deposited on a 10×10 triangular lattice.

In this paper, and in order to efficiently occupy the sites of the lattice, we randomly select empty k-tuples from the set of empty k-tuples, instead of from the whole lattice. This strategy improves significantly the computational cost of the algorithm.

3. Kinetics and jamming coverage

In order to calculate the jamming thresholds, the probability $W_L(\theta)$ that a lattice of linear size L reaches a coverage θ will be used [27]. In the simulations, the procedure to determine $W_L(\theta)$ consists of the following steps: (a) the construction of an

J. Stat. Mech. (2017) 073206

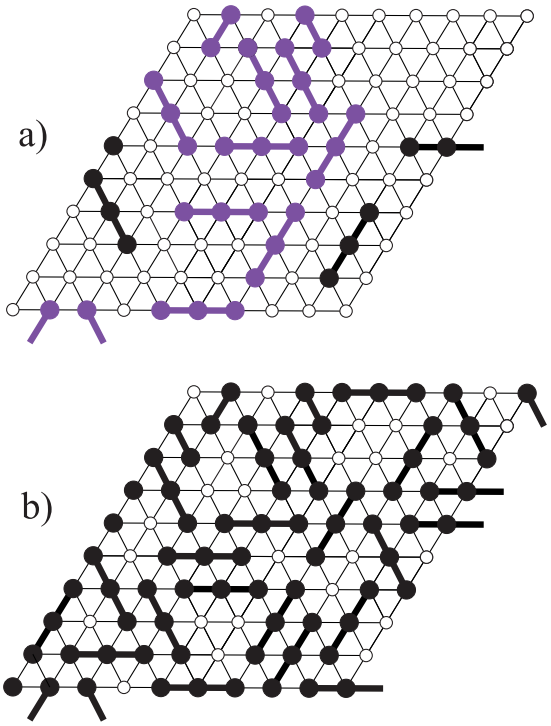

Figure 1. Typical configurations corresponding to trimers (solid circles) deposited on a 10×10 triangular lattice. Open circles denote empty sites. This particular example shows (a) the formation of a percolating cluster (highlighted in blue), and (b) the evolution of the same trial until reaching the jamming condition.

L−lattice (initially empty) and (b) the deposition of particles on the lattice up to the jamming limit θ_J. The jamming limit is reached when it is not possible to adsorb any more k-mers on the surface. A typical jamming configuration corresponding to trimers adsorbed on a 10×10 lattice is shown in figure 1(b). In the late step, the quantity $m_{\rm i}(\theta)$ is calculated as

$$m_{\rm i}(\theta) = \begin{cases} 1 & \text{for} \quad \theta \leqslant \theta_J \\ 0 & \text{for} \quad \theta > \theta_J. \end{cases} \tag{1}$$

n runs of such two steps (a) and (b) are carried out for obtaining the number $m(\theta)$ of them for which a lattice reaches a coverage θ,

$$m(\theta) = \sum_{i=1}^{n} m_{\rm i}(\theta). \tag{2}$$

Then, $W_L(\theta) = m(\theta)/n$ is defined and the procedure is repeated for different values of L. A set of $n = 10^5$ independent samples is numerically prepared for several values of the lattice size ($L/k = 100$, 150, 200, 300). The L/k ratio is kept constant to prevent spurious effects due to the k-mer size in comparison with the lattice linear size L.

For infinite systems ($L \to \infty$), $W_L(\theta)$ is a step function, being 1 for $\theta \leqslant \theta_J$ and 0 for $\theta > \theta_J$. For finite values of L, $W_L(\theta)$ varies continuously between 1 and 0, with a sharp fall around θ_J. As shown in [27], the jamming coverage can be estimated from the curves of the probabilities W_L plotted versus θ for several lattice sizes. In the vicinity

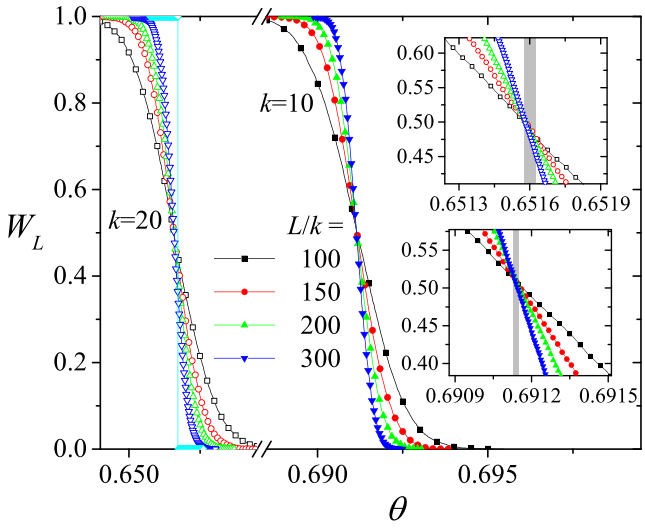

Figure 2. Curves of W_L as a function of the density θ for several values of L/k and two typical cases, $k = 10$ and $k = 20$, as indicated. Insets: Zoom of the main figure in the vicinity of the intersection points. The grey strip indicates the region where the intersections occur and their width is an estimation of the error.

of the limit coverage, the probabilities show a strong dependence on the system size. However, at the jamming point, the probabilities adopt a nontrivial value W_L^*, irrespective of system sizes in the scaling limit. Thus, plotting $W_L(\theta)$ for different linear dimensions L yields an intersection point W_L^*, which gives an accurate estimation of the jamming coverage in the infinite system.

The strategy adopted here for calculating θ_J has been successfully applied in previous studies from our group [27, 28]. The accuracy of the results obtained in [27, 28] encourage us to use this method in the present case. Similar results could be obtained by averaging over jamming concentrations for each specific lattice size L, and then extrapolating these averages.

In figure 2, the probabilities $W_L(\theta)$ are shown for different values of L/k (as indicated) and two typical cases: (a) $k = 10$ (left); and (b) $k = 20$ (right). The curves of $W_L(\theta)$ were obtained on a set of $n = 10^5$ runs. From the inspection of the figure (and from data do not shown here for a sake of clarity), it can be seen that: (a) for each k, the curves cross each other in a unique point W_L^*; (b) those points do not modify their numerical value for the different cases studied, being $W_L^* \approx 0.50$; (c) those points are located at very well defined values in the θ-axes determining the jamming threshold for each k, $\theta_{J,k}$; and (d) $\theta_{J,k}$ decreases for increasing values of k.

The procedure of figure 2 was repeated for k ranging between 2 and 128. The results are shown in figure 3 and compiled in the second column of table 1. Two well-differentiated regimes can be observed. In the range $2 \leqslant k \leqslant 20$, the values obtained of θ_J coincide with those reported in [24] and [26], and can be fitted with the function proposed in [23]: $\theta_{J,k} = \theta_0 + \theta_1 \exp(-k/r)$, with $\theta_0 = 0.684(3)$, $\theta_1 = 0.332(6)$ and $r = 2.66(2)$ (see inset). These results validate our program and calculation method.

https://doi.org/10.1088/1742-5468/aa79ae

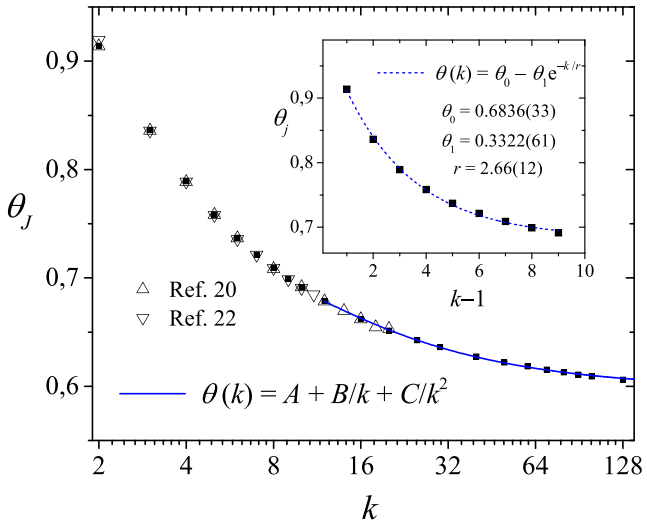

Figure 3. Jamming coverage $\theta_{J,k}$ as a function of k for linear k-mers on triangular lattices with k between 2 and 128. Inset: As main figure for $2 \leqslant k \leqslant 10$. Solid squares represent simulation results (second column of table 1), open symbols denote previous data in the literature [24, 26], and lines correspond to the fitting functions as discussed in the text.

For large values of k, the data follow a similar behavior to that predicted by Bonnier *et al* [17] for square lattices: $\theta_{J,k} = A + B/k + C/k^2 (k \geqslant 12)$, being $A = \theta_{J,k=\infty} = 0.5976(5)$ the result for the limit coverage of a triangular lattice by infinitely long k-mers, $B = 1.268(30)$ and $C = -3.61(34)$.

The value $\theta_{J,k=\infty} = 0.5976(5)$ improves the previously obtained in [24] using an exponential fit, showing the advantages of having reached larger sizes for the objects.

4. Percolation

4.1. Simulation scheme

As it was already mentioned, the central idea of percolation theory is based on finding the minimum concentration $\theta = \theta_p$ for which a cluster extends from one side of the system to the opposite. We are interested in determining *i)* the dependence of θ_p as a function of the size k, and *ii)* the universality class of the phase transition occurring in the system.

The finite-scaling theory gives us the basis to determine the percolation threshold and the critical exponents of a system with a reasonable accuracy. For this purpose, the probability $R = R^X_{L,k}(\theta)$ that an L–lattice percolates at the concentration θ of occupied sites by rods of size k can be defined [8, 29, 30]. Here, the following definitions can be given according to the meaning of X:

J. Stat. Mech. (2017) 073206

Table 1. Jamming coverage versus k. The values marked with [a] have been digitized from figure 4 of [24].

k	θ_J	θ_J ([24])	θ_J ([26])
2	0.9142(12)	0.9139(5)	0.9194(5)
3	0.8364(6)	0.8362(7)	0.8358(5)
4	0.7892(5)	0.7886(8)	0.7888(7)
5	0.7584(6)	0.758[a]	0.7579(6)
6	0.7371(7)	0.737[a]	0.7356(8)
8	0.7091(6)	0.708[a]	0.7089(8)
10	0.6912(6)	0.692[a]	0.6906(9)
12	0.6786(6)	0.678[a]	
20	0.6515(6)	0.653[a]	
30	0.6362(6)		
40	0.6276(6)		
50	0.6220(7)		
60	0.6183(6)		
70	0.6153(6)		
80	0.6129(7)		
90	0.6108(7)		
100	0.6090(8)		
128	0.6060(13)		

- $R^{x_1}_{L,k}(\theta)$: the probability of finding a percolating cluster along the x_1-direction,
- $R^{x_2}_{L,k}(\theta)$: the probability of finding a percolating cluster along the x_2-direction,
- $R^{x_3}_{L,k}(\theta)$: the probability of finding a percolating cluster along the x_3-direction,.

Other useful definitions for the finite-size analysis are:

- $R^{U}_{L,k}(\theta)$: the probability of finding a cluster which percolates on any direction,
- $R^{I}_{L,k}(\theta)$: the probability of finding a cluster which percolates in the three (x_1, x_2, x_3) directions,
- $R^{A}_{L,k}(\theta) = \frac{1}{3}[R^{x_1}_{L,k}(\theta) + R^{x_2}_{L,k}(\theta) + R^{x_3}_{L,k}(\theta)]$.

Computational simulations were applied to determine each of the previously mentioned quantities. Each simulation run consists of the following steps: (a) the construction of a triangular lattice of linear size L and coverage θ, (b) the cluster analysis using the Hoshen and Kopelman algorithm [31]. In the last step, the size of largest cluster S_L is determined, as well as the existence of a percolating island.

A total of m_L independent runs of such two steps procedure were carried out for each lattice size L. From these runs a number m^X_L of them present a percolating cluster, this is done for the desired criterion among $X = x_1, x_2, x_3, I, U, A$. Then, $R^X_{L,k}(\theta) = m^X_L/m_L$ is defined and the procedure is repeated for different values of L, θ and k.

In addition to the different probabilities $R^X_{L,k}(\theta)$, the percolation order parameter P and the corresponding susceptibility χ have been measured [32, 33],

$$P = \langle S_L \rangle / M, \tag{3}$$

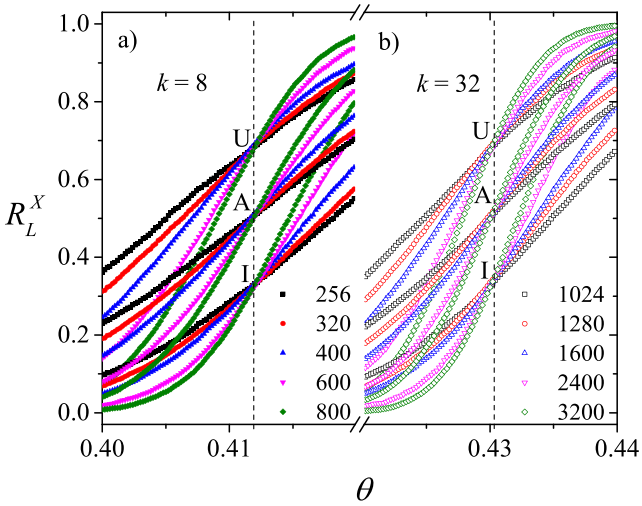

Figure 4. Fraction of percolating lattices $R^X_{L,k}(\theta)$ ($X = I, U, A$ as indicated) as a function of the concentration θ for $k = 8$ (a), $k = 32$ (b) and different lattice sizes: $L/k = 32$, squares; $L/k = 40$, circles; $L/k = 50$, up triangles; $L/k = 75$, down triangles; and $L/k = 100$, diamonds. Vertical dashed line denotes the percolation threshold $\theta_{p,k}$ in the thermodynamic limit.

and

$$\chi = [\langle S_L^2 \rangle - \langle S_L \rangle^2]/M, \tag{4}$$

where S_L represents the size of the largest cluster and $\langle ... \rangle$ means an average over simulation runs.

In our percolation simulations, we used $m_L = 10^5$. In addition, for each value of θ, the effect of finite size was investigated by examining square lattices with $L/k = 32, 40, 50, 75, 100$. As it can be appreciated this represents extensive calculations from the numeric point of view. From there on, the finite-scaling theory can be used to determine the percolation threshold and the critical exponents with a reasonable accuracy.

4.2. Percolation threshold

The standard theory of finite-size scaling [8, 29, 30] allows for various efficient routes to estimate the percolation threshold from simulation data. One of these methods, which will used here, is from the curves of $R^X_{L,k}(\theta)$.

In figure 4, the probabilities $R^I_{L,k}(\theta)$, $R^U_{L,k}(\theta)$ and $R^A_{L,k}(\theta)$ are presented for two typical cases: (a) $k = 8$ (left); and (b) $k = 32$ (right). In order to express these curves as a function of continuous values of θ, it is convenient to fit $R^X_{L,k}(\theta)$ with some approximating function through the least-squares method. The fitting curve is the *error function* because $\mathrm{d}R^X_{L,k}(\theta)/\mathrm{d}\theta$ is expected to behave like the Gaussian distribution [30]

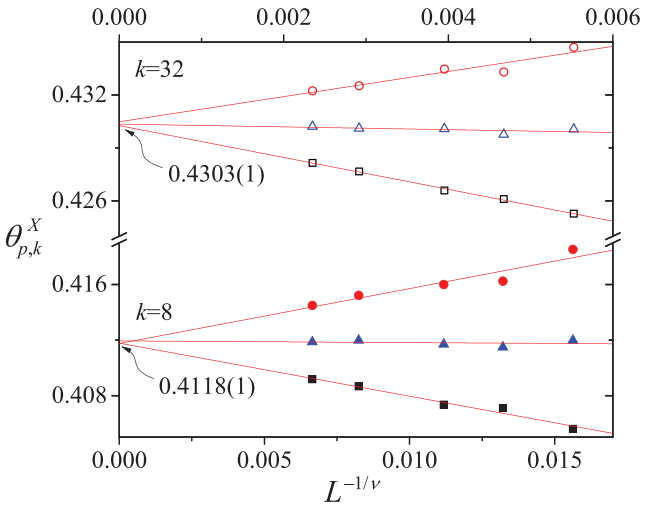

Figure 5. Extrapolation of $\theta^X_{p,k}(L)$ towards the thermodynamic limit according to the theoretical prediction given by equation (6). Circles, triangles and squares denote the values of $\theta^X_{p,k}(L)$ obtained by using the criteria I, A and U, respectively. Different values of k are presented: (a) $k = 8$ and (b) $k = 32$, and ν was taken equal to 4/3.

$$\frac{\mathrm{d}R^X_{L,k}}{\mathrm{d}\theta} = \frac{1}{\sqrt{2\pi}\Delta^X_{L,k}} \exp\left\{-\frac{1}{2}\left[\frac{\theta - \theta^X_{p,k}(L)}{\Delta^X_{L,k}}\right]\right\}, \tag{5}$$

where $\theta^X_{p,k}(L)$ is the concentration at which the slope of $R^X_{L,k}(\theta)$ is the largest and $\Delta^X_{L,k}$ is the standard deviation from $\theta^X_{p,k}(L)$.

Once obtained the values of $\theta^X_{p,k}(L)$ for different lattice sizes, a scaling analysis can be done [8]. Thus, we have

$$\theta^X_{p,k}(L) = \theta^X_{p,k}(\infty) + A^X L^{-1/\nu}, \tag{6}$$

where A^X is a non-universal constant and ν is the critical exponent of the correlation length which will be taken as 4/3 for the present analysis, since, as it will be shown in section 4.3, our model belongs to the same universality class as random percolation [8].

Figure 5 shows the plots towards the thermodynamic limit of $\theta^X_{p,k}(L)$ according to equation (6) for the data in figure 4. From extrapolations it is possible to obtain $\theta^X_{p,k}(\infty)$ for the criteria I, A and U. Combining the three estimates for each case, the final values of $\theta_{p,k}(\infty)$ can be obtained. Additionally, the maximum of the differences between $|\theta^U_{p,k}(\infty) - \theta^A_{p,k}(\infty)|$ and $|\theta^I_{p,k}(\infty) - \theta^A_{p,k}(\infty)|$ gives the error bar for each determination of $\theta_{p,k}(\infty)$. In this case, the values obtained were: $\theta_{p,k=8}(\infty) = 0.4118(1)$ and $\theta_{p,k=32}(\infty) = 0.4303(1)$. For the rest of the paper, we will denote the percolation threshold for each size k by $\theta_{p,k}$ (for simplicity we will drop the '(∞)').

The procedure of figure 5 was repeated for k ranging between 2 and 256, and the results are shown in figure 6 (solid squares) and collected in the second column of table 2. A nonmonotonic size dependence is observed for the percolation threshold, which decreases for small particles sizes, goes through a minimum around $k = 13$, and finally grows for large segments. This striking behavior has already been observed for

J. Stat. Mech. (2017) 073206

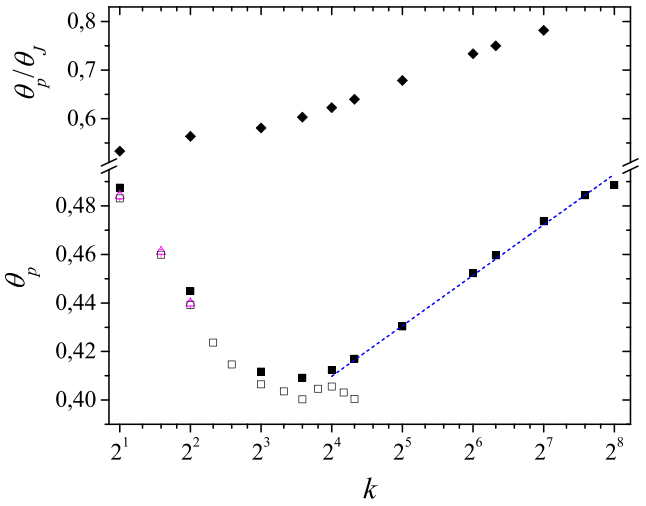

Figure 6. Squares represent the percolation threshold $\theta_{p,k}$ as a function of k for linear k-mers on triangular lattices with k between 2 and 256 (second column of table 2). Open symbols denote previous data in the literature [24]. Diamonds represent the ratio θ_p/θ_J and dashed line corresponds to the the fitting function $\theta_{p,k} = a + b \log k$.

Table 2. Percolation threshold versus k. The values marked with [a] have been digitized from figure 4 of [24].

k	θ_p	θ_p ([24])
2	0.4876(5)	0.4841(13)
4	0.4449(13)	0.4399(12)
8	0.4118(1)	0.407[a]
12	0.4092(5)	0.400[a]
16	0.4124(6)	0.406[a]
20	0.4169(3)	0.401[a]
32	0.4303(1)	
64	0.4523(4)	
80	0.4597(3)	
128	0.4737(8)	
192	0.4844(5)	
256	0.4887(7)	

the percolation threshold of k-mers on square lattice [17, 20, 21], and can be interpreted as a consequence of the local alignment effects occurring for larger k (long needles) and their influence on the structure of the critical clusters [17, 21].

We tried to fit the obtained data for larger k ($k = 16...256$), using the function $\theta_{p,k} = a + b \log k$, being $a = 0.3265(26)$ and $b = 0.030\,03(70)$. In figure 6 can also be observed the ratio of percolation and jamming concentrations, θ_p/θ_J, which shows a monotonically increasing behavior. Combining the fitting functions used for both concentrations we obtain an estimation for this ratio which increases, for large k, proportionally to $\log k$. In this way, the condition $\theta_p/\theta_J \simeq 1$ corresponds to a value of $k \simeq 10^4$ from which percolation would no longer occur. Similar result has been obtained in the case of straight rigid rods on a square geometry [21, 22]. In [22], the authors determined

J. Stat. Mech. (2017) 073206

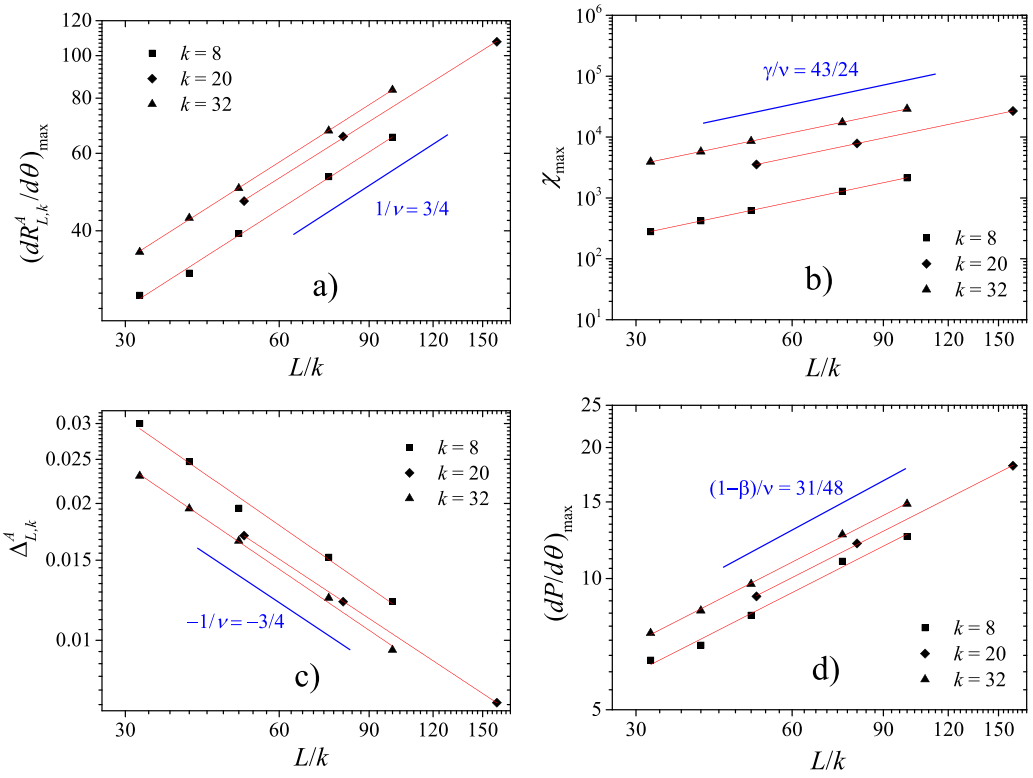

Figure 7. (a) Log–log plot of $\left(dR^A_{L,k}/d\theta\right)_{\max}$ as a function of L/k for $k = 8$ (squares), $k = 20$ (diamonds) and $k = 32$ (triangles). According to equation (7) the slope of each line corresponds to $1/\nu = 3/4$. (b) Log–log plot of $\chi_{\max}$ as a function of L/k and the same values of k. The slope of each line corresponds to $\gamma/\nu = 43/24$. (c) Log–log plot of $\Delta^A_{L,k}$ as function of L/k. (d) Log–log plot of $(\mathrm{d}P/\mathrm{d}\theta)_{\max}$ as a function of L/k. According to equation (10), the slope of each curve corresponds to $(1-\beta)/\nu = 31/48$.

that the percolation phase transition only exists for values of k between 1 and approximately 6×10^3. For $k > 6 \times 10^3$, percolation cannot occur, even at (maximal) jamming concentration.

4.3. Critical exponents and universality class

In this section, the critical exponents ν, β and γ will be calculated. Critical exponents are of importance because they describe the universality class of a system and allow for the understanding of the related phenomena.

The standard theory of finite-size scaling allows for various methods to estimate ν from numerical data. One of these methods is from the maximum of the function in equation (5) [8],

$$\left(\frac{\mathrm{d}R^X_{L,k}}{\mathrm{d}\theta}\right)_{\max} \propto L^{1/\nu}. \tag{7}$$

In figure 7(a), $\ln\left[\left(\mathrm{d}R^{A}_{L,k}/\mathrm{d}\theta\right)_{\max}\right]$ has been plotted as a function of $\ln[L]$ (note the log–log functional dependence) for $k=8$, $k=20$ and $k=32$. According to equation (7) the slope of each line corresponds to $1/\nu$. As it can be observed, the slopes of the curves remain constant (and close to 3/4) for all studied cases. Thus, $\nu=1.36(3)$ for $k=8$; and $\nu=1.35(2)$ for $k=32$. The results coincide, within numerical errors, with the exact value of the critical exponent of the ordinary percolation $\nu=4/3$.

Another alternative way of evaluating ν is given through the divergence of the standard deviation of the threshold observed from their average values, $\Delta^{X}_{L,k}$ in equation (5),

$$\Delta^{X}_{L,k} \propto L^{-1/\nu} \tag{8}$$

Figure 7(c) shows $\ln\left[\Delta^{X}_{L,k}\right]$ as a function of $\ln[L]$ (note the log–log functional dependence) for $k=8$, 20 and 32. According to equation (8), the slope of each line corresponds to $1/\nu$. As in figure 7(a), the slopes of the curves remain constant and close to $-3/4$.

Once we have ν, the exponent γ can be determined by scaling the maximum value of the susceptibility equation (4). According to the finite-size scaling theory [8], the behavior of χ at criticality is $\chi=L^{\gamma/\nu}\overline{\chi}(u)$, where $u=(\theta-\theta_{p,k})\,L^{1/\nu}$ and $\overline{\chi}$ is the corresponding scaling function. At the point where χ is maximal, $u=$const. and $\chi_{\max}\propto L^{\gamma/\nu}$. Our data for $\chi_{\max}$ are shown in figure 7(b). The values obtained are $\gamma=2.35(1)$ for $k=8$ and $\gamma=2.38(1)$ for $k=32$. Simulation data are consistent with the exact value of the critical exponent of the ordinary percolation, $\gamma=43/18$.

On the other hand, the standard way to extract the exponent ratio β is to study the scaling behavior of P at criticality [8],

$$P=L^{-\beta/\nu}\overline{P}\,(u')\,, \tag{9}$$

where $u'=|\theta-\theta_{p,k}|L^{1/\nu}$ and $\overline{P}$ is the scaling function. At the point where $\mathrm{d}P/\mathrm{d}\theta$ is maximal, $u=$const. and

$$\left(\frac{\mathrm{d}P}{\mathrm{d}\theta}\right)_{\max}=L^{(-\beta/\nu+1/\nu)}\overline{P}\,(u')\propto L^{(1-\beta)/\nu}. \tag{10}$$

The scaling of $(\mathrm{d}P/\mathrm{d}\theta)_{\max}$ is shown in figure 7(d). From the slopes of the curves, the following values of β were obtained: $\beta=0.18(2)$ for $k=8$ and $\beta=0.19(4)$ for $k=32$. These results agree very well with the exact value of β for ordinary percolation, $\beta=5/36=0.14$.

The protocol described in figure 7 was repeated for k between 2 and 128. In all cases, the values obtained for ν, γ and β clearly indicate that, independently of the size k, this problem belongs to the same universality class that the random percolation. This finding is expected, given the robustness of this universality for RSA models like the one studied in this paper [16, 19, 34–37].

The scaling behavior can be further tested by plotting $R^{X}_{L,k}(\theta)$ versus $(\theta-\theta_{p,k})\,L^{1/\nu}$, $PL^{\beta/\nu}$ versus $|\theta-\theta_{p,k}|L^{1/\nu}$ and $\chi L^{-\gamma/\nu}$ versus $(\theta-\theta_{p,k})\,L^{1/\nu}$ and looking for data collapsing [8] see supplementary material[4].

[4] See supplemental material (stacks.iop.org/JSTAT/2017/073206/mmedia) for the details on the data collapsing tests.

J. Stat. Mech. (2017) 073206

5. Conclusions

In this paper, extensive numerical simulations and finite-size scaling theory have been used to study the percolation properties of straight rigid rods of length k out of equilibrium (RSA adsorption) as well as the jamming threshold on the two-dimensional triangular lattice.

A nonmonotonic size dependence was found for the percolation threshold θ_p, which decreases for small particles sizes, goes through a minimum around $k = 13$, and finally increases for large segments. The behavior observed for small values of k had already been described by Budinski-Petković *et al* [24]. However, the increase of θ_p for large values of k is reported here for the first time in a triangular geometry. This striking behavior, also observed for square lattices [17, 21], is related to local alignment effects that affect the structure of the percolation cluster. In fact, compact blocks of oriented k-mers are formed on the surface for large values of k, and the system behaves qualitatively similar to an ideal RSA of k-blocks, where the percolation threshold increases with k [38].

On the other hand, the observed functionality of the jamming coverage with k suggests that percolation is impossible if k exceeds approximately 10^4. For $k > 10^4$, percolation cannot occur, even at (maximal) jamming concentration. Similar conjecture has been proposed for the case of straight rigid rods on square lattices, where the limit value of k leading to percolation is approximately 6×10^3 [22]. The existence of this limit object size can also be understood from the interplay between percolation and jamming effects in a RSA model of k-blocks [38]. However, more simulations are necessary in order to obtain direct confirmation of this conjecture for straight rigid k-mers.

Finally, we observe that the nature of the phase transition occurring in the system is not affected, belonging to the same universality class of the ordinary random percolation.

Acknowledgments

This work was supported in part by CONICET (Argentina) under project number PIP 112-201101-00615; Universidad Nacional de San Luis (Argentina) under project 03-0816; and the National Agency of Scientific and Technological Promotion (Argentina) under project PICT-2013-1678. The numerical work were done using the BACO parallel cluster (composed by 50 PCs each with an Intel i7-3370 / 2600 processor) located at Instituto de Física Aplicada, Universidad Nacional de San Luis—CONICET, San Luis, Argentina.

References

[1] Erban R and Chapman S J 2007 *Phys. Rev.* E **75** 041116
[2] Evans J W 1993 *Rev. Mod. Phys.* **65** 1281
[3] Privman V 2000 *Colloids Surf.* A **165** 231
[4] Senger B, Voegel J C and Schaaf P 2000 *Colloids Surf.* A **165** 255
[5] Talbot J, Tarjus G, Van Tassel P R and Viot P 2000 *Colloids Surf.* A **165** 287
[6] Cadilhe A, Araújo N A M and Privman V 2007 *J. Phys.: Condens. Matter* **19** 065124

J. Stat. Mech. (2017) 073206

[7] Zallen R 1983 *The Formation of Amorphous Solids, in The Physics of Amorphous Solids* (Weinheim: Wiley-VCH) (https://doi.org/10.1002/3527602798.ch1)
[8] Stauffer D and Aharony A 1994 *Introduction to Percolation Theory* (Boca Raton, FL: CRC Press)
[9] Sahimi M 1994 *Applications of Percolation theory* (Boca Raton, FL: CRC Press)
[10] Grimmett G 1999 What is Percolation?, *in Percolation* (Berlin: Springer)
[11] Bollobás B and Riordan O 2006 *Percolation* (Cambridge: Cambridge University Press)
[12] Krapivsky P L, Redner S and Ben-Naim E 2010 *A Kinetic View of Statistical Physics* (Cambridge: Cambridge University Press)
[13] Bunde A, Harder H and Dieterich W 1986 *Solid State Ion.* **18–19** 156
[14] Harder H, Armin Bunde and Dieterich W 1986 *J. Chem. Phys.* **85** 4123
[15] Evans J W 1987 *J. Phys. A: Math. Gen.* **20** 6487
[16] Evans J W and Sanders D E 1989 *Phys. Rev.* B **39** 1587
[17] Bonnier B, Hontebeyrie M, Leroyer Y, Meyers C and Pommiers E 1994 *Phys. Rev.* E **49** 305
[18] Vandewalle N, Galam S and Kramer M 2000 *Eur. Phys. J.* B **14** 407
[19] Cornette V, Ramirez-Pastor A J and Nieto F 2003 *Eur. Phys. J.* B **36** 391
[20] Kondrat G and Pękalski A 2001 *Phys. Rev.* E **63** 051108
[21] Tarasevich Y Y, Lebovka N I and Laptev V V 2012 *Phys. Rev.* E **86** 061116
[22] Tarasevich Y Y, Laptev V V, Vygornitskii N V and Lebovka N I 2015 *Phys. Rev.* E **91** 012109
[23] Budinski-Petković L and Kozmidis-Luburić U 1997 *Phys. Rev.* E **56** 6904
[24] Budinski-Petković L, Lončarević I, Petković M, Jakšić Z M and Vrhovac S B 2012 *Phys. Rev.* E **85** 061117
[25] Budinski-Petković L, Lončarević I, Jakšić Z M, Vrhovac S B and Švrakić N M 2011 *Phys. Rev.* E **84** 051601
[26] Budinski-Petković L, Lončarević I, Jakšić Z M and Vrhovac S B 2016 *J. Stat. Mech.* 053101
[27] García G D, Sanchez-Varretti F O, Centres P M and Ramirez-Pastor A J 2015 *Physica* A **436** 558
[28] Centres P M and Ramirez-Pastor A J 2015 *J. Stat. Mech.* P10011
[29] Binder K 1997 *Rep. Prog. Phys.* **60** 487
[30] Yonezawa F, Sakamoto S and Hori M 1989 *Phys. Rev.* B **40** 636
[31] Hoshen J and Kopelman R 1976 *Phys. Rev.* B **14** 3438
[32] Biswas S, Kundu A and Chandra A K 2011 *Phys. Rev.* E **83** 021109
[33] Chandra A K 2012 *Phys. Rev.* E **85** 021149
[34] Dolz M, Nieto F and Ramirez-Pastor A J 2005 *Eur. Phys. J.* B **43** 363
[35] Lebrecht W, Valdés J F, Vogel E E, Nieto F and Ramirez-Pastor A J 2013 *Physica* A **392** 149
[36] Lebrecht W, Valdés J F, Vogel E E, Nieto F and Ramirez-Pastor A J 2014 *Physica* A **398** 234
[37] Longone P, Centres P M and Ramirez-Pastor A J 2012 *Phys. Rev.* E **92** 011108
[38] Nakamura M 1987 *Phys. Rev.* A **36** 2384

J. Stat. Mech. (2017) 073206